DOI: 10.1021/ma902797f

Macromolecules
ARTICLE

Conformational Heterogeneity in PNA:PNA Duplexes

Filbert Totsingan,[†,‡,§,#] Vipul Jain,[‡,#] W. Clay Bracken,[⊥] Andrea Faccini,[§] Tullia Tedeschi,[§] Rosangela Marchelli,[§] Roberto Corradini,*[,§] Neville R. Kallenbach,*[,†] and Mark M. Green*[,‡]

[†]*Department of Chemistry, New York University, 100 Washington Square East, New York, New York 10003,* [‡]*Herman F. Mark Polymer Research Institute, Polytechnic Institute of New York University, 6 MetroTech Center, Brooklyn, New York 11201,* [§]*Dipartimento di Chimica Organica ed Industriale, Università di Parma, Via G.P. Usberti 17/A, 43100 Parma, Italy, and* [⊥]*Department of Biochemistry, Weill Medical College of Cornell University, 1300 York Avenue, New York, New York 10021.* [#] *These coworkers contributed equally.*

Received December 18, 2009; Revised Manuscript Received February 4, 2010

ABSTRACT: Oligomers of PNA:PNA duplexes with different amino acids appended to one strand of each duplex have been synthesized and studied for their chiral optical properties. The terminal amino acid is known to affect both the handedness and amplitude of the CD signal from a given duplex. Here we have investigated an extended set of duplexes with several different amino acids appended, determining the CD, absorbance, and denaturation behavior of these chains in water and glycerol. Thermal unfolding profiles of the duplexes together with NMR data point to conformational heterogeneity as a function of amino acid, oligomer length, and solvent. The results suggest that the PNA:PNA double helix has access in solution to a dynamic ensemble of conformational states rather than a single dominant state. The conformational ensemble varies as a function of oligomer length according to the cooperative properties of the competing conformations of the double helix. A simplified statistical theoretical model allowing only two conformational states with distinct cooperative properties consistent with the denaturation results can account for much of the experimental data. This conformational heterogeneity in PNA duplexes is reflected in significantly greater flexibility of PNA:DNA duplexes relative to either DNA or RNA double helices. The results demonstrate that the principles of chiral cooperativity such as seen in the sergeants and soldiers and majority rule experiments must be altered when the structure of the system becomes a variable depending on the chiral information input.

Introduction

Structural studies are of fundamental importance in understanding the function of nucleic acids in biological systems and are an essential element of modern DNA nanotechnology.[1] DNA is able to adopt many different structures, which are the result of different balance in the fundamental features of base pairing (hydrogen bonding) base stacking, internal stereochemical constraints, and external constraint due to solvent or DNA-binding molecules. The variety of possible DNA conformations is still under investigation, and several questions remain to be addressed, such as the nature of the intermediate state observed in stretching studies of DNA.[2]

One source of information in this field may come from variants of DNA in which some of the structural features (e.g., stereochemistry, sugar, or nucleobase structures) are either chemically changed or reduced in their complexity.[3] Peptide nucleic acids (PNAs) are oligonucleotide analogues, composed of *N*-(2-aminoethyl)glycine monomers linked to nucleobases through a carboxymethylene linker (Figure 1). Because of the lack of the deoxyribose cyclic structure, the steric constraint in each repeating unit is reduced and stereochemical bias is eliminated. Furthermore, the polyamide backbone is neutral, and therefore repulsive interactions between negatively charged phosphate groups are lacking.[3,4] In spite of these severe changes, PNAs are able to bind cDNA and RNA with high affinity and selectivity[5] and have been used in biomedical applications, such as in diagnostics[6] or in the development of gene therapeutic agents based on antisense[7−10] or antigene strategies.[11,12]

Interestingly, PNA:PNA duplexes can also be formed as DNA-like double helices, suggesting that a helical structure can simply be obtained by the combination of hydrogen bonding and base stacking interactions even in the presence of a less constrained and more flexible backbone lacking of electrostatic repulsive forces.[13−15] The PNA double helix has a higher melting temperature than the corresponding PNA:DNA and DNA:DNA,[16−18] suggesting that the stabilizing interactions are much less affected by other destabilizing effects.

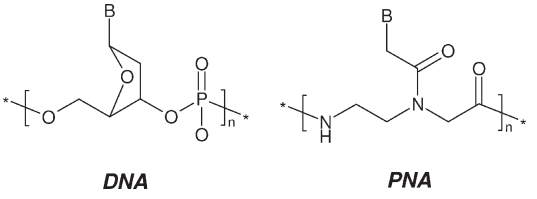

Figure 1. Schematic structures of PNA and DNA.

In stereochemically unbiased PNA:PNA duplexes, equal amounts of left- and right-handed helices have been observed,[18,19] with a conformation which differs from DNA:DNA duplexes in terms of helical pitch (18 bp) but which has a similar rise (3.2 A vs 3.4 A for DNA) allowing base stacking to occurr effectively.

A systematic modulation of helix handedness in PNA:PNA duplexes can be obtained by means of modified PNA structures in which stereochemical bias has been introduced.[20] The preference of one handedness derived from a chiral PNA backbone was shown to modulate the DNA binding ability by inducing helical preorganization.[21] Flexible, acyclic PNA molecules, with side chains derived from amino acids (such as lysine or alanine), were shown to produce a control of PNA:PNA helix handedness depending on the stereochemistry of the monomeric units. It was shown that the influence on helix handedness is

*To whom correspondence should be addressed. E-mail: mgreen@duke.poly.edu (M.M.G.); nrk1@nyu.edu (N.R.K.); roberto.corradini@unipr.it (R.C.).

 Published on Web 02/19/2010

Table 1. PNA Oligomers Sequences Used in the Present Study

duplex	chiral PNA[a]	complementary strand
6-aa	H-ATCTAC-aa-NH_2	H-GTAGAT-NH_2
8-aa	H-TGATCTAC-aa-NH_2	H-GTAGATCA-NH_2
10-aa	H-AGTGATCTAC-aa-NH_2	H-GTAGATCACT-NH_2
12-aa	H-ACAGTGATCTAC-aa-NH_2	H-GTAGATCACTGT-NH_2
15-aa	H-GTGACAGTGATCTAC-aa-NH_2	H-GTAGATCACTGTCAC-NH_2
17-aa	H-CTGTGACAGTGATCTAC-aa-NH_2	H-GTAGATCACTGTCACAG-NH_2
19-aa	H-ATCTGTGACAGTGATCTAC-aa-NH_2	H-GTAGATCACTGTCACAGAT-NH_2

[a] aa = C-terminal amino acid (L-Lys, L-His, L-Arg).

stronger if the chiral monomers are placed in the middle of the PNA strands.[22,23] The effects of the configurations of chiral monomers with stereocenters at both C2 or C5 have been thoroughly investigated and rationalized.[24]

Preferential helicity of PNA:PNA duplexes, which is otherwise racemic, can also be induced by conjugation of chiral amino acids at the C-terminus of one of the two PNA strands, as shown in early works by Nielsen and co-workers.[18,25] In particular, lysine flanked by one GC base pair affects the helical handedness of the PNA:PNA duplexes, as measured by circular dichroism studies.[25] In this case, the initial stereochemical bias is propagated through the PNA:PNA duplex by the cooperative interactions that induce the helical conformation, with a propagation of chirality of the "sergeant and soldiers" type.[26] These chiral optical observations have been assumed to be related to an excess helical handedness of the duplex arising from the chiral influence of the appended amino acid. Early studies of the effect of a terminal lysine in a series of PNA duplexes with varying chain lengths led to the conclusion that the chiral influence of the lysine extends only as far as the tenth base pair, at which point a loss of stereochemical bias was supposed to occur, leading to constant CD signals.[25] This result suggested a limit in the cooperative properties of PNA duplexes, namely that after 10 base pairs the chiral bias of base stacking interactions is too attenuated to prevent a reversal of the double-helical sense.

Surprisingly, in the solid state the preference for one handedness has not been observed, as the stability of the racemate in the unit cell far overwhelms the chiral influence of the terminal amino acid.[27] The preference for the racemate crystals even under the influence of chiral information that causes a large excess of one helical sense in solution has also been observed in vinyl polymers in early works by the Italian school of polymer science.[26b,28]

The present work extends the studies of the effect of terminal amino acids on the PNA double helix by varying the appended amino acids and using longer oligomers than previously studied.[25] Circular dichroism (CD), nuclear magnetic resonance (NMR), and melt data monitored by ultraviolet (UV) hypochromicity as well as the temperature dependence of chiral optical signals show that the terminal amino acids affect the PNA duplex beyond simply controlling the handedness of the duplex. The appended amino acid affects the duplex structure distal to the point of attachment of the amino acid as a consequence of an extended range of conformational states in solution with a population which depends on both the amino acid and the oligomer length of the duplex.

The length dependence of the CD signal from different amino acids in particular shows complex behavior, consistent with a structural model in which an ensemble of PNA duplex conformations differ as a function of the terminal amino acid, suggesting that the PNA duplex itself is intrinsically conformationally heterogeneous, rather than possessing the unique helical structure observed in the solid state.[19,27] Appending an amino acid may stabilize and restrict this conformational manifold to a smaller set, but the system remains multistate in nature. These results reinforce and extend conclusions gained from a crystallographic study of partially self-complementary PNA showing that the PNA duplex structure can form several types of hydrogen-bonding schemes[29] and shed new light on the conformational heterogeneity of PNA:PNA duplexes.

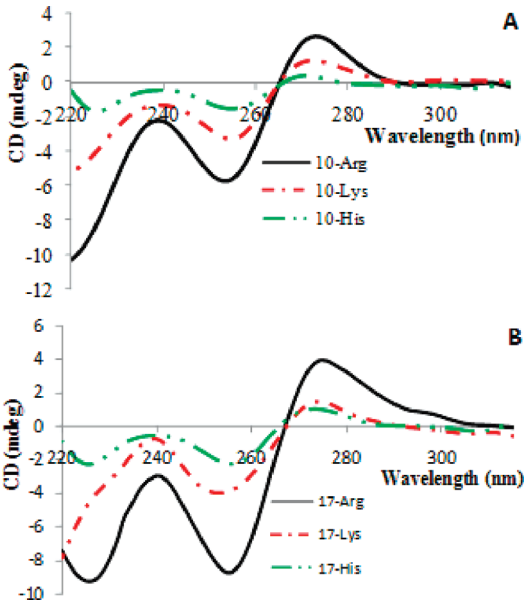

Figure 2. CD spectra of 10 base pairs (A) and 17 base pairs (B) PNA:PNA duplexes. All spectra were recorded in water (pH 6.8) at T = 22 °C. Duplex concentration = 5 μM.

Results

Length and Solvent Dependence of CD and UV Spectra of PNA:PNA Duplexes. A series of PNAs of different lengths and with different types of L-amino acids directly linked at the C-terminus was synthesized, as reported in Table 1. In the series of data here considered, cationic amino acid side chains were chosen on the basis of earlier observations indicating a larger effect on PNA:PNA helicity handedness. For each amino acid-terminated oligomer, the corresponding complementary PNA strand was synthesized allowing formation of antiparallel duplexes.[18,22,30] If the amino acid's effect defined only the handedness of the produced double helix, the sign and intensity, but not the shape, of the CD spectra of the oligomers would vary as a function of amino acid. A change in shape of the CD spectra, if observed, would point to conformational changes in the PNA duplex. Consistent with conformational states that are affected by the terminal amino acid, in addition to the ratio of left- and right-handed forms, the CD spectral shapes do differ in the low wavelength region for the PNA duplexes studied. As an example of our findings, Figure 2 exhibits results for the 10-mer and 17-mer of three different amino acid-terminated PNA duplexes.

Figure 3A exhibits the normalized CD amplitudes at the wavelength maxima (molar CD divided by the number of bases) for each oligomer, for the lysine-, arginine-, and

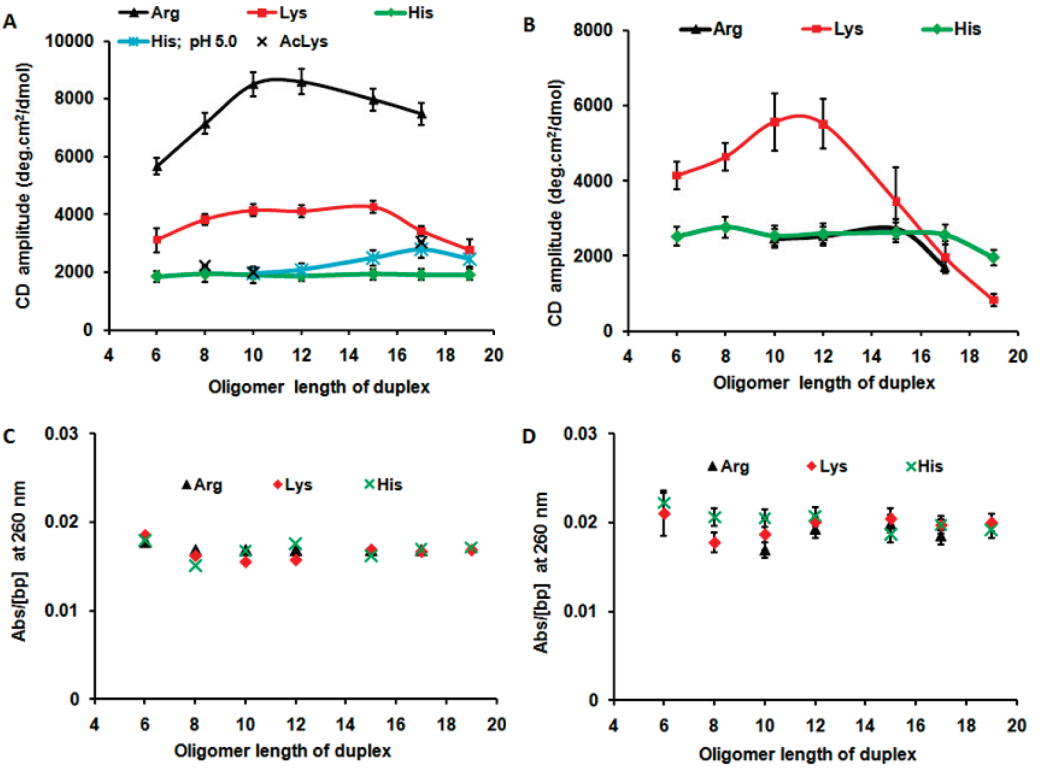

Figure 3. Molar ellipticity (deg cm^2 dmol^{-1}) and UV absorbance (260 nm) per base pair as a function of oligomer length of PNA:PNA duplexes in water pH 6.8 (A, C) and glycerol/water (9:1) mixture (B, D). The CD amplitude ($\theta_{275} - \theta_{255}$) was normalized by bases concentration. T = 22 °C. Duplex concentration = 5 μM. Each data point was obtained by averaging the amplitude of two different samples containing the same duplex, and the error bars are defined on the basis of the related standard deviation.

histidine-terminated PNA duplexes in water. Figure 3B shows a parallel data set for the same three duplexes in a mixture of 90% glycerol and 10% water.

In the absence of any conformational change as a function of the terminal amino acid, for each amino acid as oligomer length increases, constant values, hence lines of zero slope, should result for each of the three terminal amino acid duplexes studied in each solvent. This observation is expected since the only change among the amino acids and the different oligomer lengths would be the ratio of the left- and right-handed double helices. The ratio of left- and right-handed helices should be independent of oligomer length if there are no conformational changes as a function of oligomer length. A flat line is, in fact, seen for the case of the histidine-terminated PNA duplex in water, but only at the higher pH, and not in the mixed solvent for this amino acid. In the arginine- and lysine-terminated duplexes, slope changes with increasing oligomer length occur in both solvent systems. Importantly, the three duplexes with differing terminal amino acids exhibit different slopes of CD intensity per base versus oligomer length in the two solvent systems. The elimination of the possibility of solubility as the explanation for the results in Figure 3A,B is demonstrated by the regularity of the absorbance data of the duplexes plotted against chain length in both solvent systems (Figure 3C,D). The UV absorbance, which is associated with the hypochromicity arising from base stacking,[31−34] shows only small differences pointing to differing base stacking properties as a function of chain length for the differing amino acid-terminated oligomeric double helices. The results in Figure 3 demonstrate that the three duplexes with differing terminal amino acids differ from each other beyond simply the ratio of left- to right-handed double-helical conformations. Moreover, oligomers of each individual amino acid-terminated duplex differ from each other as well. The structural changes called for by these observations (Figure 3A,B) are, surprisingly, only reflected in the low wavelength shape of the CD spectra for the various duplexes in each solvent (Figure 2) and are only weakly reflected in the hypochromicity data (Figure 3C,D).

The CD signal is also strongly affected by the solvent, since both the intensity and the length dependence are different going from pure water to 9:1 glycerol/water mixture. This effect is particularly large in the case of Arg, with a net decrease of the CD signal per base pair. In the case of Lys, the solvent effect shifted the maximum CD per base pair to shorter oligomers and a strong decrease of the CD intensity for the longer oligomers. The pH of the solution also plays a role in the amino acid−PNA interactions in the case of His, for which lowering the pH from 7 to 5 (thus increasing the positive charge on the side chain) resulted in a different length dependence of the CD signal, with stronger signals for the pH = 5 case. The use of ε-acetylated lysine as terminal amino acid for 8-, 10-, and 17-mer oligomers further confirmed the solvent dependence, and the results show a reduced CD signal (crosses in Figure 3A) and the absence of a horizontal relationship for the three oligomers measured.

Temperature Dependence of CD and UV Absorption. Conformational distinctions among the various amino acid appended PNA duplexes, as demonstrated by the results in Figures 2 and 3 should lead to different melting properties as a function of the different appended amino acid. Melting data are known to be exceptionally sensitive to the twist and tilt properties associated with the base pairs (B-DNA vs Z-DNA).[35] Melting experiments were therefore conducted based on the fact that dissociation of a PNA duplex is accompanied by increase in UV absorbance, hyperchromism,

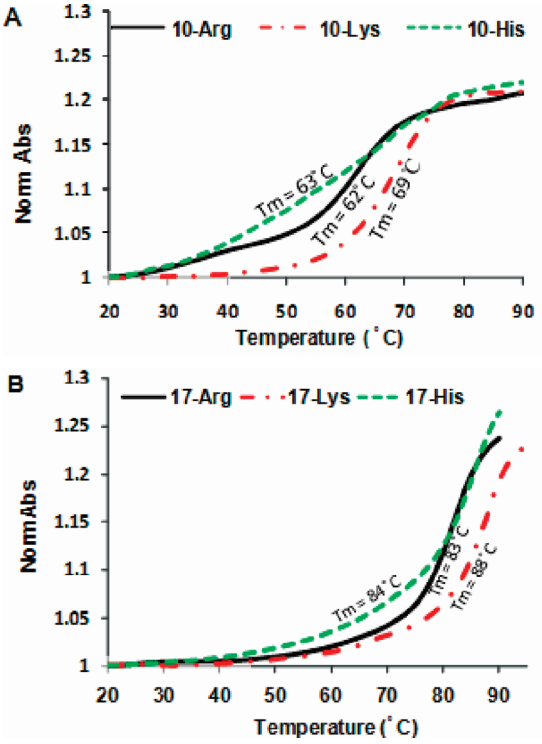

Figure 4. UV melting profiles of 10 base pairs (A) and 17 base pairs (B) PNA:PNA duplexes. All spectra were recorded in water (pH 6.8). Duplex concentration = 5 μM.

Table 2. UV Melting Temperatures of PNA:PNA Duplexes in Water

	terminal amino acid (aa), T_m (°C)		
PNA duplex	Lys	His	Arg
6-aa	33	28	29
8-aa	55	53	53
10-aa	69	63	62
12-aa	75	72	72
15-aa	84	77	78
17-aa	88	84	83
19-aa	91	85	n.d

arising from loss of base stacking, parallel to observations long known for DNA duplex melting.[36]

As illustrated by the two examples in Figure 4 and the complete data set in Table 2, the duplexes are fully formed at 22 °C with the melting temperature increasing with the length of the oligomers, thus showing that the terminal amino acid clearly affects the melting and therefore the thermodynamic stability of the duplex. Since not only the melting temperature but also the shapes of the curves were different with different amino acids, the amino acid−PNA interaction induces differences which are reflected in the entire structure by affecting the base stacking, which propagates throughout the duplex.

The melting data for lysine, arginine, and histidine confirm that the results in Figure 3 arise from differing conformational states. Moreover, the apparent T_m values (the midpoint of the absorbance profiles) indicate that the histidine- and arginine-terminated duplexes are less stable than the lysine ones (Table 2).

Additional information related to the unfolding data can be gained by studying the temperature dependence of the CD intensity. Since chiral control must originate at the base pairs flanking the amino acid site, and since loss of CD intensity can occur via disruption of either the helical conformation or base pairing/stacking before the global single stranded states are populated, the CD unfolding profiles should be completed before the full hyperchromism develops, that is, at temperatures below the T_m of the duplex. These data are shown in graphical form for the lysine- and histidine-terminated duplexes in Figure 5. Complete $T_{1/2}$ data are summarized in Table 3. Comparison of the data in Tables 2 and 3 shows that the predicted effect is indeed observed and moreover that the temperature difference for melting of the duplex versus loss of the CD signal increases with oligomer length. Therefore, by comparison of the CD and UV melting temperature, we can asses that two processes are occurring: (1) loss of optical activity, which is measured by CD, and (2) dissociation of the two PNA strands, which is measured by UV hyperchromicity. These two are not clearly distinguishable at short oligomer length due to the small differences between T_m and $T_{1/2}$ but can clearly be detected at longer oligomer lengths (17−19), for which the melting temperature is increased much more than the $T_{1/2}$. As an example, the Lys containing 17-mer PNA:PNA duplex at 85 °C is less than half dissociated (Figure 4B), but the CD signal is already completely lost (Figure 5D).

It is interesting to note that the process leading to the loss of CD signal is different for the two amino acids Lys and His in the case of 10-, 15-, and 17-mer, with that of His-PNA decreasing earlier than that of the Lys·PNA, thus suggesting that at least the terminal part of the helix is stabilized by interactions occurring with the Lys moiety.

^{1}H NMR Studies. Since the results presented above point clearly to conformations that depend on the identity of the terminal amino acid, we verified if this behavior could be confirmed by NMR study of the hydrogen bonding between the bases on the two strands. For reasons of solubility and spectral resolution this effort was restricted to ^{1}H NMR spectroscopy of a series of hexamer duplexes terminated by lysine, arginine, and histidine. The 6-mer length allows resolution of distinct imino proton signals at low field corresponding to individual base pairs in each duplex. Assignment of peaks was carried out using 2D NOESY (as reported in the Supporting Information). The resonances are numbered from the amino acid site as follows

aa-*C*1*A*2*T*3*C*4*T*5*A*6

*G*1*T*2*A*3*G*4*A*5*T*6

with the ring NH containing bases indicated in boldface.

The differing NMR spectra, taken at 7 °C, shown in Figure 6, support the conclusion that the terminal amino acid influences the structure of the PNA duplexes at sites distal from the substitution site. In each case, the downfield peak near 14 ppm corresponds to the ring NH of T6, as demonstrated by this peak being first to disappear at increasing temperature, arising from increase in fraying at the chain end, which also causes the relative invariance of the chemical shift of this peak. The furthest upfield peak near 12 ppm is the ring NH of G1 (as deduced from intrastrand NOESY peaks with a flanking thymine residue, Supporting Information). The remaining peaks that cluster between 13 and 13.4 ppm include the ring NH of G4, T2, T3, and T5. The chemical shift of the latter series varies with the amino acid among the hexamers. Although the main peak for G1 shows only a small variation among the hexamers, the shoulder on the high field side of this peak resolves into different peaks at higher temperature pointing to differing conformations of the base pairing. The lysine hexamer reveals more than one conformation, since there are other small broad peaks in the spectrum, consistent with the previous observation in a lysine terminated PNA palindromic octamer.[37] At low

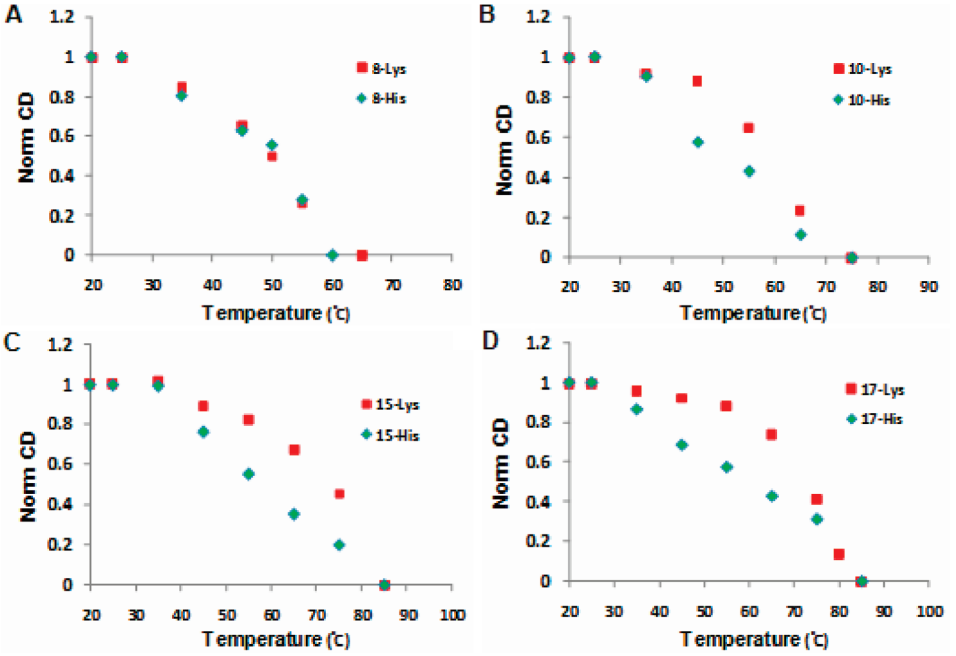

Figure 5. Sample CD melting profiles for lysine (red) and histidine (green) terminated duplexes: 8 base pairs (A), 10 base pairs (B), 15 base pairs (C), and 17 base pairs (D) PNA:PNA duplexes. All spectra were recorded in water (pH 6.8). Duplex concentration = 5 μM.

Table 3. CD Melting Temperatures ($T_{1/2}$(CD))[a] of PNA:PNA Duplexes in Water

	terminal amino acid (aa), $T_{1/2}$(CD) (°C)	
PNA duplex	Lys	His
6-aa	27	25
8-aa	53	50
10-aa	60	55
12-aa	65	58
15-aa	75	60
17-aa	78	65
19-aa	78	70

[a] Corresponds to the loss of 50% of the initial CD signal.

temperature, the variation of the signal positions points at a different ensemble of conformations in rapid exchange on the NMR time scale. Whereas the small signal must be due to conformations in slow exchange with the predominant one, the weak intensity of these peaks did not allow characterization of these minor species.

Analysis of the NMR spectra of the Arg-terminated hexamer at different temperatures showed that disappearance of the imino protons did not occur simultanously, with the T6 signal disappearing before the other thymines, while the G1 signal was the most persistent one. These results indicate the presence of an additional interaction which prevented fraying on the side of the helix bearing the amino acid (Figure 7). This observation clearly shows that there is a direct interaction of the amino acid side chain with the adjacent base pair in solution, though it was not observed in the solid state.[27] This in turn is in agreement with the effect of the terminal amino acid on the melting temperature and on CD intensity reported above.

Thus, the present NMR data reveal that the chemical environment (hence their chemical shift) of the nucleobases distant from the amino acid (in particular from T2 to T5) is different depending on the terminal amino acid used. These results are compatible with the interpretation that the amino acids do not affect solely the terminal base pair, but the entire duplex overall conformation.

Discussion

Following the pioneering work of Nielsen's group,[25] the double-helical duplexes formed by complementary pairs of PNA strands reveal interesting chiral properties as discussed in the Introduction. In this work[25] and in much research[27,38,39] that followed their initial effort, the effects of terminal amino acids have been assumed to control helical handedness within a conformational double-helical structure that is predominantly unaffected by the amino acid. X-ray crystallographic studies have pointed to a double helix[27] with the general assumption made that a similar conformation would apply in the dissolved state. A recent NMR study of a PNA:PNA duplex with a symmetric sequence was interpreted similarly, although in the structure studied the presence of two terminal lysine units may act to enhance the structural rigidity.[37]

As noted in the Introduction, an amino acid-terminated PNA duplex that shows a CD signal in solution indicating an excess of one helical sense nevertheless crystallizes with *both* helical senses of the duplex equally populated, parallel to observations on single-strand-helical synthetic polymers.[26b,28] This phenomenon, arising from the usually higher melting point of crystals of racemates, demonstrates that the effect of the amino acid on the PNA system is strongly dependent on the environment: the chiral control of the amino acid can be overcome by crystal packing effects. The observation suggests that crystallographic helical parameters for PNA duplexes may not necessarily reflect solution phase conformational states.

In the data reported here, as discussed in the Results section, we find that the terminal amino acid exerts more than a chiral effect. Instead, each amino acid induces changes in the structural parameters of the PNA:PNA duplex that extend considerably beyond the point of attachment of the amino acid, indeed out to chain lengths of 19 base pairs and probably beyond, although longer oligomers were not synthetically accessible in this study.[40]

Two main observations can be derived from the CD data: (i) the intensity of the CD signal is dependent on the amino acid used, on the chain length, and on the solvent; (ii) the dependence of the CD signal on chain length is different from amino acid to

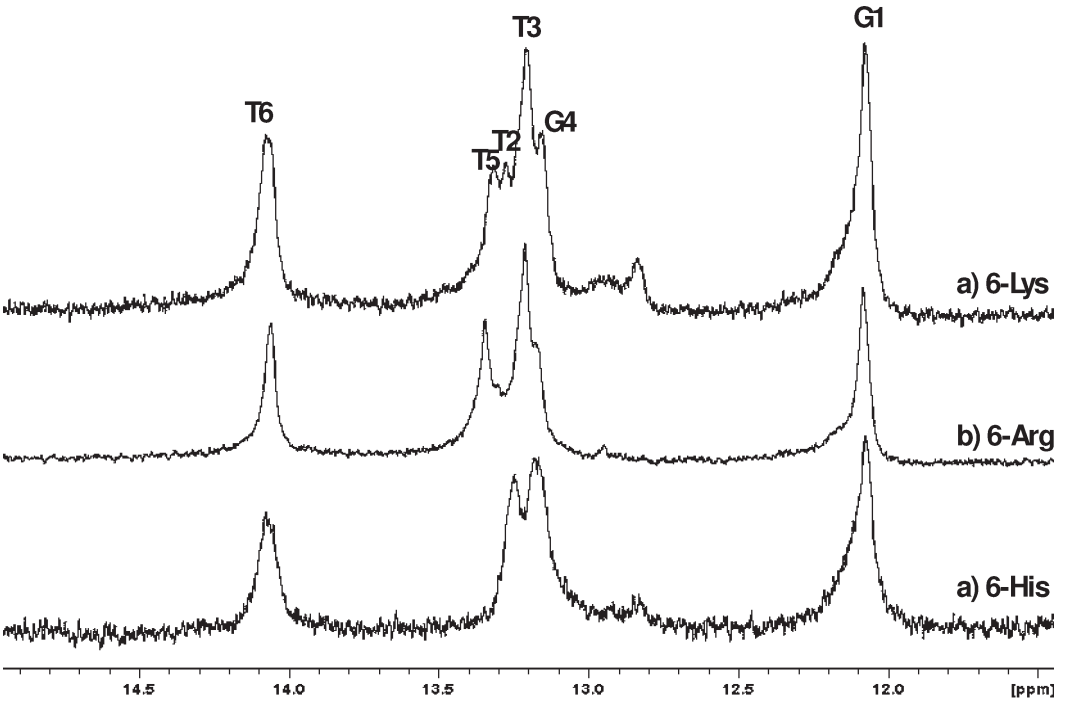

Figure 6. ^{1}H NMR spectra of the imino protons region of the six base pairs PNA:PNA duplexes terminated with (a) L-lysine, (b) L-arginine, and (c) L-histidine. All spectra were recorded at 7 °C in H_2O/D_2O (9:1), pH 7.1, 20 mM sodium phosphate buffer. Duplex concentration = 0.9 mM.

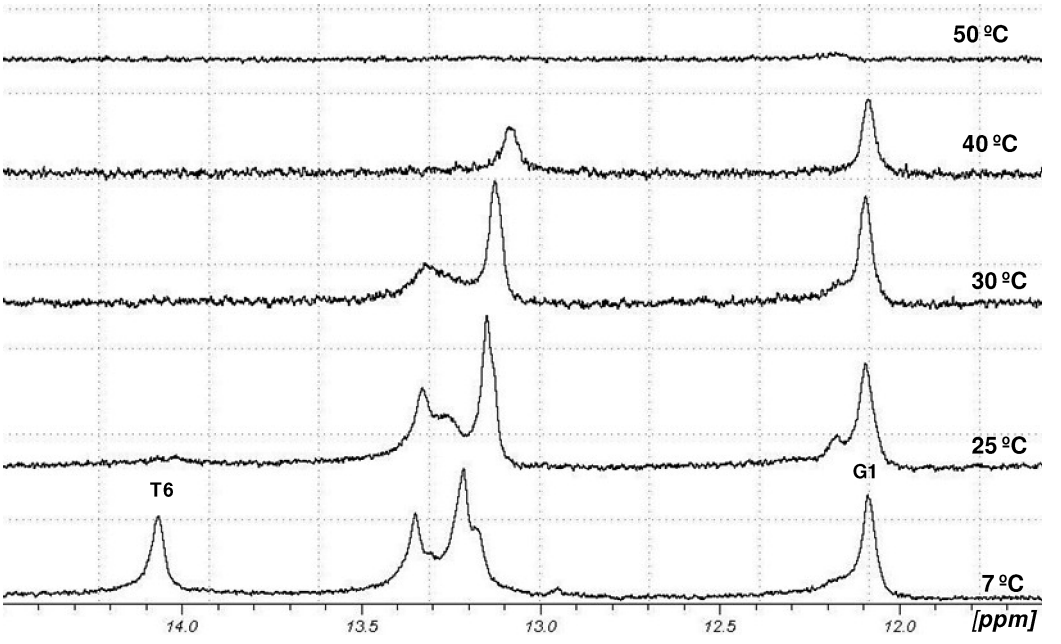

Figure 7. ^{1}H NMR spectra of the imino protons region of the six base pairs PNA:PNA duplex terminated with L-arginine at different temperatures.

amino acid and is not constant as a function of oligomer length when calculated as contribution per base pair. Therefore, there is a strong connection between the terminal amino acid and the overall duplex conformation since the spectroscopic properties (CD intensity, melting data, and NMR chemical shifts) are dependent on the type of the amino acid also for base pairs distant from the amino acid itself. The terminal amino acid therefore affects not only the helical handedness but also the collective behavior of the bases as a function of length.

The data in Figure 3 are particularly striking. In water (pH 6.8), the lysine- and arginine-terminated duplexes show large changes in slope over a range of oligomer lengths, while the histidine system only shows these changes in slope at lower pH (5.0). In glycerol/water, the changes in slope of the molar ellipticity as a function of oligomer length are still more obvious for the lysine- and arginine-terminated duplexes, while the uncharged histidine-terminated duplex in this mixed solvent now exhibits a slope change leading to a *decrease* in CD molar ellipticity at higher degree of oligomerization. These data are unexpected in light of the traditional assumption of a single conformational state. However, the effect has proven highly reproducible after repeated experiments on independent samples synthesized and measured in different laboratories involved in this effort.

The temperature dependence of the CD intensity reported in Figure 5 clearly shows a differential effect of the two terminal amino acids (lysine and histidine) on the CD signal as a function of the temperature. In the case of histidine the loss of CD signal occurs gradually, whereas the lysine system shows greater cooperativity. From the data in Tables 2 and 3, $T_{1/2}$ is always lower than T_m. Because the two amino acids must interact differently with the flanking GC base pair, the qualitative difference in the effect of temperature on the CD intensity behavior could reasonably be connected to the strength of the base pairing at the C-terminus and not necessarily to the effect of the amino acids on the conformational properties of the duplex distal to the amino acid. However, as discussed below, the results in Figure 5 prove valuable in supporting the multistate model when correlated with a quantitative theoretical model.

The salient conclusions from our experimental observations can be summarized:

1. The CD molar ellipticity data as a function of oligomer length in two solvent systems (Figure 3A,B) implicate conformational differences in the helix geometry of duplexes terminated by each amino acid. These differences vary with oligomer length for each amino acid. This conclusion is required by the slope changes seen in Figure 3A,B. If a single conformational state applies to the PNA duplex, independent of the terminal amino acid and of oligomer length, one should expect the slopes of the CD molar ellipticity per base as a function of oligomer length at temperatures below T_m to be flat for all the amino acid-terminated PNA duplexes, differing only in magnitude along the ordinate.

2. The melting data for the three terminal amino acids (Figure 4) require that the amino acid affects the stability of the duplex over a range of distances from the point of attachment of the amino acid; that is, the cooperativity changes with each amino acid.

3. The NMR data (Figures 6 and 7) for double-helical 6-mers are consistent with heterogeneous conformational properties as a function of the terminal amino acid.

4. The thermodynamic stabilities of the duplexes (Table 2) do not correlate with the amplitude of the associated CD spectra. Thus, the extent of helix excess is unrelated to the stability of the duplex, which we expect to be related to base pair−base pair stacking effects as in DNA duplexes.

5. The CD spectra for different amino acids differ in the low wavelength regions indicating distinct conformational features. Small changes are also seen in the hypochromicity data as a function of terminal amino acid and degree of oligomerization, leading to the same conclusion.

A two-state model analysis of melting data such as those reported in Figure 4 was performed (Supporting Information, Table S3), indicating that not only differences in short oligomers were observed, which were attributable to end effect of the amino acid (stabilizing or destabilizing the first base pair), but also that both enthalpy and entropy contributions changed as a function of the terminal amino acid when adding bases not immediately adjacent to the amino acid itself; for example, the calculated enthalpy gain going from 10-mer to 15-mer, i.e., by adding five bases at the end opposite to that of the amino acid, was of 28 kcal mol^{-1} for Lys, 51.3 kcal mol^{-1} for Arg, and 37 kcal mol^{-1} for His. Comparison with the achiral PNA:PNA (for the 10-mer case) was also provided: in this case the $-\Delta H°$ varied in the following order: His < Arg < Achiral < Lys, whereas the $-\Delta S°$ values follow the opposite order showing enthalpy−entropy compensation. However, a more elaborated analysis had to be used to account for all the above-reported effect, including CD melting experiments.

The experimental data cannot be reconciled with a model in which the terminal amino acid affects only the left- and right-handed states of the double helix or with a model in which a single distinct oligomer independent conformational state can be assigned to each amino acid. Moreover, if two states with identical conformations differ only in handedness (e.g., with the PNA tract either right- or left-handed), their ratio as a function of oligomer length must be fixed. This would lead to a constant CD signal per base or at least to leveling off once a defined length is reached. Finally, one conformational state interrupted by helical reversals that appear beyond a critical oligomer length cannot fit the data, since this effect should occur at the same PNA length for all amino acids.

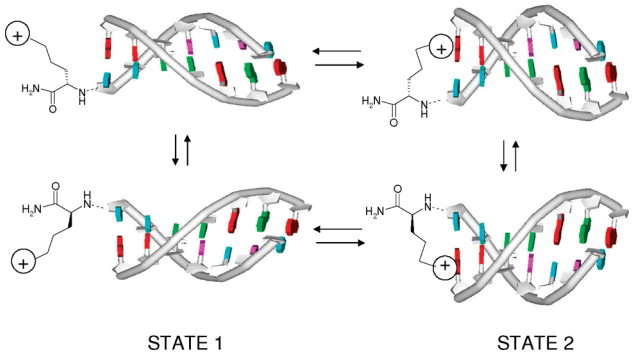

Figure 8. Schematic representation of multistate model. Only two states (1 and 2) with different cooperativity parameters are considered for simplicity. The terminal amino acid can stabilize one of the two handednesss and one of the two states by interaction with the terminal base.

To understand the experimental observations, we are forced to propose conformational heterogeneity by assuming that there is an ensemble of differing conformations (at least two) for each duplex whose population is a function of both the terminal amino acid and the oligomer length. Each appended amino acid, in this model, interacts with the adjacent base pair in multiple ways. These interactions guide distinct conformations accessible to the duplex giving rise to multiple states along the length of the duplex, which then account for the chiral optical, hypochromicity, melt, and NMR data.

Each of the multiple states, for example differing in the twist and tilt properties of the base pairs and in the conformation of the backbone, can reasonably be expected to be distinct in its cooperative properties as depicted in Figure 8. If the amino acid give rise to a stronger interaction with the first base pair, it can shift the equilibrium toward a more cooperative state (in Figure 8 indicated as state 2). For each amino acid the conformational ensemble will vary as a function of oligomer length since the effect of the amino acid distal to the point of attachment is determined by the cooperative interactions within that particular conformational state. As a result, the CD spectrum for each oligomer length for each amino acid reflects an average of different chiral conformations, which means that the overall CD can vary with oligomer length.

The manifold, in principle, can include chains with either right- or left-handed helical sense (as indicated in Figure 8) although the contribution of a nonhelical conformation (such as that proposed for DNA[41]) cannot be ruled out.

Since the presence of the amino acid affects the population of the various states and not their nature, which is determined by the states compatible with the PNA duplex structure, we can conclude that this "multistate" can also be present in naked PNA. Unfortunately, since the naked PNA has no chiral bias, CD experiments would give no evidence for this.

To put this picture on a more quantitative basis, we have applied a simple statistical thermodynamic description of the PNA−PNA duplex based on similar theories of the melting transition in short heterogeneous DNA duplexes (see Methods

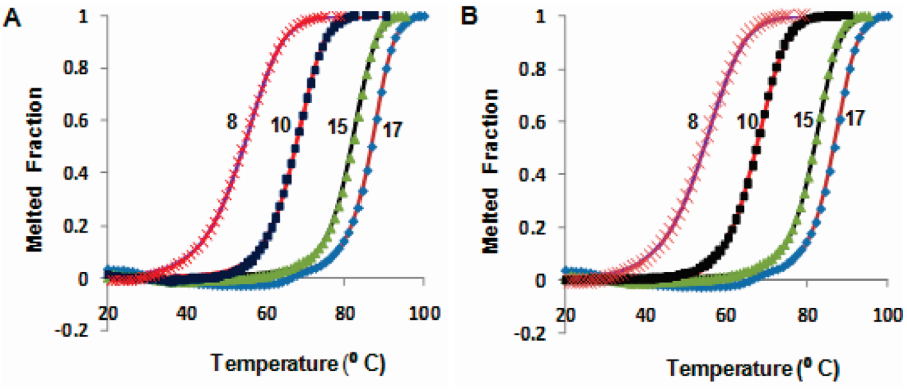

Figure 9. Experimental and fitted melting curves of 8-, 10-, 15-, and 17-mer PNA:PNA duplexes with a C-terminal lysine. Solid curves are calculated using (A) $\gamma = 10^{-8}$ and (B) $\gamma = 10^{-10}$. Experimental data are shown by symbols.

section and Supporting Information). We have applied, as a minimalist model, this theoretical description to the lysine- and histidine-terminated oligomeric PNA duplexes assuming only two sets of underlying substructures. We sought to determine whether this kind of theory in this limited form can account for the experimental data available, in particular the experimental loss of CD intensity with temperature (Figure 5) and the slope changes with oligomer length seen in Figure 3A,B. Success in even approximately fitting such an oversimplified model to the any of the amino acid data sets would demonstrate the applicability of the model to all the PNA duplexes studied here and by implication to any amino acid-terminated PNA duplex.

The theoretical modeling was carried out, in detail, with the following assumptions (for simplicity): only two conformational sets of duplex helical substructures are allowed, which melt to a common single-stranded population. Each double-helical substructure is characterized by distinct fraying properties at its C and N termini. Fraying at the aminoacyl terminus results in a zero contribution to the CD. Loss of other base pairing reduces the CD contribution in proportion to the number of base pairs opened. Each set of states is governed by a fixed nucleation constant, together with different stabilities for the AT and GC base pairs present. Normalizing the overall ensemble CD intensity allows comparison with normalized values of the experimental CD data, facilitating comparison between the two.

The two proposed states (Figure 8) differ, as noted above, in their conformational properties, including (undefined) twist and tilt angles of the base pairs and their differing propensity for fraying at either the C or N terminus. Cooperativity parameters, consistent with the melt data in Figure 4, for the two duplex conformational states are $\gamma_1 = 10^{-8}$ (state 1) and $\gamma_2 = 10^{-10}$ (state 2). The fit of the theory to the UV melt data for the three amino acid-terminated double helices using these cooperativity parameters lead to average values for base pairing enthalpy and entropy: $(\Delta H_1, \Delta S_1) = (-8690, -22.02)$; $(-8170, -20.77)$; $(-6400, -15.70)$ cal mol^{-1} bp^{-1} for lysine, arginine, and histidine in state 1, respectively, and $(-8320, -20.16)$; $(-7870, -19.07)$; $(-6140, -14.10)$ cal mol^{-1} bp^{-1} for lysine, arginine, and histidine in state 2, respectively. Therefore, the terminal amino acid not only gives rise to interactions which add a contribution to the overall enthalpy but also affects the entropy of base−base interactions.

These thermodynamic values afford precise fits to the temperature-dependent absorbance profiles for the three amino acid-terminated PNA duplexes similar to that shown in Figure 9 for the lysine-terminated PNA duplex. The fitting results in Figure 9 show that both γ_1 and γ_2 values are consistent with the experimental data, provided that the thermodynamic parameters are adjusted accordingly.

On the assumption that the CD signal results from at least two intact flanking base pairs, the same parameters could be used to fit the CD melt data. The experimental data for lysine-terminated duplexes are shown in Figure 5. Figure 10 compares the theoretical with the experimental results, the latter shown as red symbols in the figure. The green and blue lines in Figure 10 correspond to the calculated change of CD intensity for each of the two structural states discussed above. The solid red line is the average of the two theoretical lines (blue and green) and makes an excellent fit to the experimental red points for the 8- and 10-mers. Considering the simplification from using only two sets of double-helical structures, the fit to the experimental data for two of the oligomers, the 8-mer and 10-mer, is reasonable, in agreement with the fact that loss of optical activity in these cases is concomitant with melting.

However, for longer oligomers, we note that the fit then falls off especially for the mid-temperature range far from the unbroken double helix and near to the fully melted state. This is precisely the region where the contribution of larger numbers of conformational states in these longer oligomers can be expected to play a larger role. Since the model used only takes into account cooperativity, it is possible that for longer oligomers structures with different conformational properties but similar cooperativity contribute to the overall CD profile, an effect which cannot be evaluated by the UV vs temperature profile alone.

Since PNA strands are more flexible than DNA, we believe that additional intermediate states are populated in longer duplexes, including internally opened states,[42] or partially inverted helical states, such as those observed in helical polymers.[26] The lack of fit between theory and experiment seen in the longer oligomers (Figure 10C,D) supports the idea that more than two states, that is, multistate models, would be required to capture additional features of the thermal unfolding profiles of the PNA duplexes. More accurate fits would include structures that are peculiar to PNA strands that would broaden the CD profiles relative to the hyperchromicity data.

In accord with our data, a manifold of different substructures actually exists, which dynamically interchange on different time scales. The NMR data in Figure 6 for example suggest that at least two different populations can be detected on a millisecond time scale at low temperature (6-Lys, an additional peak at 12.85 ppm). Further experiments would need to be performed to define the kinetics as well as the distribution of states in the NMR spectrum.

As noted above, this calculation method was applied to both the histidine- and arginine-terminated duplexes using the same cooperativity parameters, and in both cases excellent fits to the UV melt were obtained. However, the thermodynamics parameters differ from each amino acid to another.

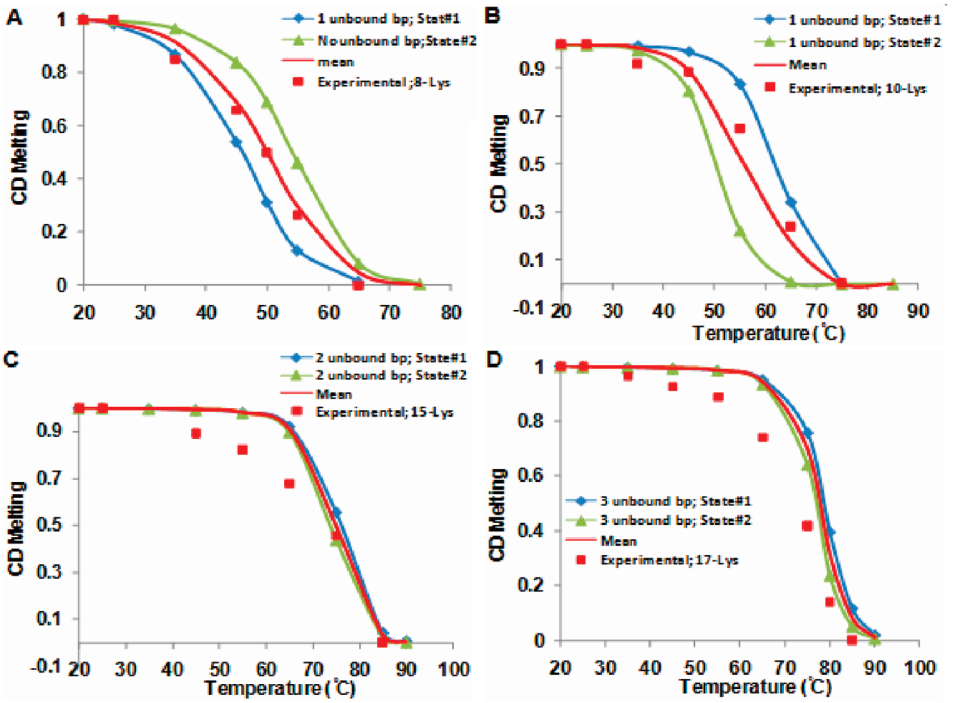

Figure 10. CD melting curves: 8-Lys (A), 10-Lys (B), 15-Lys (C), and 17-Lys (D) PNA:PNA duplexes. The mean fitting curves (solid red) is obtained as the arithmetic mean of the two states.

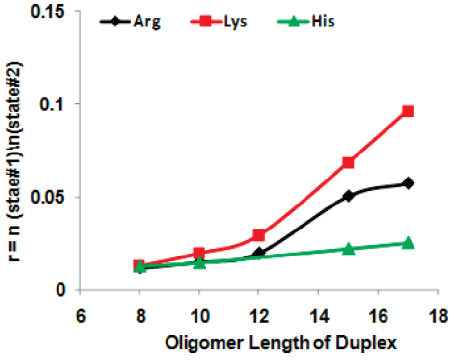

Figure 11. Boltzmann distribution of the two states populations as a function of oligomer length of PNA:PNA duplexes. As the chain length increases, the less cooperative state (state 1) becomes increasingly populated.

Using the above hypothesis, and the thermodynamic parameters thus calculated, we can predict that the population of two different states can effectively vary with the oligomer length (Figure 11). In this model, taking into account only two cooperative factors $\gamma_1 = 10^{-8}$ (state 1) and $\gamma_2 = 10^{-10}$ (state 2), the enthalpic and entropic parameters obtained from the UV melt fitting were then used to evaluate the relative population of the two "states" as a function of oligomer length for all three amino acids in aqueous solution at ambient temperature. The results of this calculation are shown in Figure 11 and reveal that clear differences in the behavior of the three amino acids can be accounted for by considering only the differences in their thermodynamic properties. In the case of histidine, the ratio of the two populations is almost constant (as observed experimentally); in this case one state largely prevails over the other. The arginine and lysine series show a strong dependence of the populations on oligomer chain length. As the chain length increases, the less cooperative state (state 1) becomes increasingly populated. By allowing that this state has a negative contribution to the CD intensity, this would cause a decrease in CD as observed in Figure 3A for the longer oligomers. This effect is more pronounced in the case of lysine-terminated duplexes as observed.

By assigning appropriate values to the CD contributions of the two substates depicted, one could, in principle, produce a change in slope in the overall CD signal at any desired chain length. Our point is that models more complex than this minimal "two double-helix states model" can readily fit the UV and CD unfolding profiles as well as the CD dependence on chain length.

In conclusion, the picture that results from these considerations obviously has sufficient degrees of freedom to explain a variety of effects. However, the fits that result from this highly simplified two substructures model are constrained by the combined thermal and CD unfolding profiles as well as the length-dependent CD data. Any realistic simulation of PNA:PNA duplex structure should reveal a highly dynamic and fluctuating ensemble of conformations, unlike the corresponding DNA:DNA or DNA:PNA duplexes.[13] This has been detected in the crystal structure of a partly self-complementary PNA reported by Petersson et al.[29] and in the recent NMR study of the palindromic PNA octamer.[37]

The knowledge of these states could be important in revealing PNA-specific motifs. We have shown that at least three parameters (terminal constraint, solvent, and temperature) can be used to control the conformational population, giving rise to different overall structures.

As a final note, the results of the study reported here show that the application of the principles of chiral cooperativity,[26] leading to amplification of chirality such as seen in the sergeants and soldiers and majority rules experiments, which are widely applicable and ranging from dynamically racemic helical arrays[43] to supramolecular helices,[44] and even to two-dimensional chiral systems,[45] cannot be directly used for situations where the structural characteristics of the system become a variable depending on the input of the chiral information as encountered here. Liquid crystals provide another example of this limitation where the chiral information changes the characteristics of the phase, at first from nematic to cholesteric and then within the cholesteric phase by change of pitch.[46]

Methods

PNA Oligomers Synthesis. Boc- and Fmoc-protected PNA monomers A, C, G, and T were purchased from Applied Biosystems and used without further purification. Boc- and Fmoc-protected L-amino acids were obtained from Novabiochem and used without further purification. PNA oligomers were synthesized by standard Boc[47] or Fmoc[48] solid-phase synthesis protocols using MBHA and Rink amide resin, respectively, and HBTU as activating reagent and *N,N*-diisopropylethylamine as base. The synthesis was performed on an ABI 433A peptide synthesizer (Applied Biosystems) with software modified to run the PNA synthetic steps. The standard small scale (5 μmol) cycles were used. The resin was first swollen for 1 h with dichloromethane and downloaded manually with L-amino acids (chiral oligomers) or with a PNA monomer (complementary sequences). The Boc-deprotection step was performed using trifluoroacetic acid (TFA)/*m*-cresol mixture (95:5). The Fmoc group of the Rink-amide resin and the growing peptide chain was removed by treatment with 20% of piperidine in DMF (2 × 8 min). Upon completion of the last monomer coupling, PNA oligomers were manually cleaved from the resin using TFA/TFMSA(trifluoromethanesolfonic acid)/*m*-cresol/thianisole mixture (6:2:1:1) for Boc synthesis or TFA/*m*-cresol (9:1) for Fmoc synthesis and precipitated with ethyl ether. The crude PNAs were purified by reversed phase HPLC with UV detection at 260 nm. A semiprep scale C18 silica column (5 μm particle size, 250 × 10 mm, Jupiter Phenomenex, 300 A) was utilized, eluting with water +0.1% TFA (eluent A) and a 60:40 mixture of water and acetonitrile + 0.1% TFA (eluent B). A linear gradient of 0−40% of B in 30 min was used at a flow rate of 4 mL/min. The resulting PNA oligomers were characterized by electrospray ionization mass spectrometry (ESI-MS) and gave positive ions consistent with the final products in each case.

Measurement of PNAs Concentration. The concentrations of the stock PNA solutions were measured using a Cary-50 UV−vis spectrophotometer (Varian) using the following protocol.[49] 10 μL of each of the stock solution was transferred to a polypropylene tube, and the weight of the solution transferred was noted. To this was transferred 750 μL of water and 250 μL of methanol. The corresponding weights were noted. The actual volumes thus transferred were calculated on the basis of density of each solvent at room temperature on that particular day. Using these volumes, the precise dilutions could be calculated by using the following equation:

$$D = [(W\rho)_{\text{water}} + (W\rho)_{\text{MeOH}}]/[W_{\text{PNA stock solution}}\,\rho_{\text{water}}]$$

D, W, and ρ denote dilution, weight, and density, respectively (of the required solvent).

The resulting mixture was transferred to a 1 cm path length UV cell, and using an external water bath, the sample was heated to 60 °C for 5 min. The UV spectrum was scanned from 400 to 200 nm, and absorbance was noted at 260 nm. The experiment was repeated for another set of similar solutions. Average of the two results was considered to get the molar concentrations of the stock solutions. Concentrations were determined by UV absorbance at 260 nm (60 °C) using the following extinction coefficients: $A = 13\,700$, $C = 6600$, $G = 11\,700$, and $T = 8600\ \text{M}^{-1}\ \text{cm}^{-1}$.

Circular Dichroism and UV Absorbance Measurements. CD measurements were performed in water (pH = 6.8, with one exception) or in water/glycerol mixture (9:1) using circular dischroism spectrometers JASCO J710 and J715 with temperature control. 1 mL PNA−PNA duplex solutions (5 μM) were prepared from the stock solutions by diluting them with the required solvent. In order to get the exact duplex concentration, all the solutions were prepared in a 2 mL Eppendorf tube by weighing the required amounts of PNA stock solutions and the solvents. The total volume and hence the precise concentration of the duplex were then calculated. The resulting samples were incubated at 90 °C for 5 min and then slowly cooled to room temperature. In the case of glycerol, after incubation, the samples were kept at room temperature overnight in order to obtain homogeneous solutions. CD spectra were recorded in triplicate from 315 to 220 nm. Each spectrum was zeroed, smoothed, and treated with a noise reduction software. The experiment was repeated twice in order to evaluate the standard deviation.

The temperature dependence of the CD spectra was carried out by increasing the temperature from 20 to 90 °C every 10 °C.

UV absorbance at 260 nm was measured for each PNA−PNA duplex solution.

UV Melting Analysis. All UV melting experiments were performed in water (pH = 6.8) or in water/glycerol mixture (9:1). An equal amount of the two complementary PNA strands was dissolved in the required solvent. Strand concentrations were 5 μM in each component. Thermal denaturation profiles (abs vs T) of the PNA−PNA duplexes were measured at 260 nm with an UV/vis Lambda Bio 20 spectrophotometer equipped with a Peltier temperature programmer PTP6 which is interfaced to a personal computer. The temperature was increased from 10 to 20 to 90 °C at a rate of 0.5 °C/min, and the UV absorbance was recorded every 0.5 °C. A melting curve was recorded for each duplex. The melting temperature (T_m) was determined from the maximum of the first derivative of the melting curves.

^{1}H NMR Experiments. NMR spectra of 6-mer PNA duplexes were recorded at 280 K on a Bruker Avance DMX-500 operating at 500.20 MHz. All experiments were performed in H_2O/D_2O (9:1) with WATERGATE water suppression. PNA duplexes concentration was 0.9 mM, and 512 scans have been collected for each ^{1}H NMR spectrum. The temperature dependence of the imino proton resonances was performed by increasing the temperature in the range 7−50 °C. The NOESY WATERGATE experiment has been performed in H_2O/D_2O (9:1). A total of 128 scans and 512 t_1 increments with mixing time of 200 ms were collected. The data were processed using TopSpin 1.3 Pl 8.

Theoretical Model and Calculations: Model. To analyze the experiment results and predict a number of important peculiarities of conformational transformations, we used the model theory developed by Crothers et al. (1965) and by Applequist et al. (1965).[50] The model takes into account (a) the disordering of end parts of double-stranded molecules (end fraying) and (b) strand dissociation once the duplex is fully melted. In a system of interacting nucleobases strands with the chain ends opposite each other (nonstaggering zipper model), the binding constant can be expressed as

$$K = \beta L(s) \tag{1}$$

β is the so-called nucleation (association) parameter and s is the base pairing constant determined by the expression

$$\ln s = -\left(\frac{\Delta H_1}{R}\right)\frac{1}{T} + \frac{\Delta S_1}{R} \tag{2}$$

In practice, we introduce two base pairing constants: one for AT pairs s_1 and one for GC pairs s_2 (Crothers et al., 1965). In the case of double-stranded molecules of length N, with n bonded base pairs, the partition function can be given by

$$L(s) = \sum_{n=1}^{N}(N-n+1)s^n \tag{3}$$

The fraction of bonded base pairs can be expressed as

$$f = \frac{s[1+4\gamma L(s) - (1+8\gamma L(s))^{1/2}]L'(s)}{4\gamma N L(s)^2} \tag{4}$$

where $L'(s)$ is the first derivative of $L(s)$ and $\gamma = \beta C$, the cooperativity parameter, with C being the total strand concentration.

Calculation Method. To fit the model to experimental data, the upper and lower segments of the melting profiles were fitted first, by assuming that the absorbance varies linearly with temperature:

$$A_s = m_s T + b_s \quad (5)$$

$$A_d = m_d T + b_d \quad (6)$$

where A_s and A_d refer to single and double strands, respectively.

f can be related to the UV absorbance (A) by the following expression:

$$f = \frac{A_s - A}{A_s - A_d} \quad (7)$$

The bonded fraction f is a function of s and γ, according to eq 4. For trial values of γ, representing different states, then s was obtained at each experimental temperature by using eq 4. ΔH_1 and ΔS_1 were then obtained by a least-squares fit of the data to eq 2.

Acknowledgment. The research leading to the results reported here was initiated in the doctoral thesis of Vipul Jain, Polytechnic University (now Polytechnic Institute of New York University), 2006, and continued in the doctoral thesis of Filbert Totsingan, University of Parma, 2008. Both Dr. Jain and Dr. Totsingan have contributed equally to the work. The effort at the Polytechnic Institute of New York University and New York University was supported by the Office of Naval Research (N.R.K.) and the National Science Foundation (M.M.G.).

Supporting Information Available: Calculation details and thermodynamic data; NMR assignment of G1 imino proton. This material is available free of charge via the Internet at http://pubs.acs.org.

References and Notes

(1) (a) Seeman, N. C. *Annu. Rev. Biophys. Biomol. Struct.* **1998**, *27*, 225–248. (b) Brucale, M.; Zuccheri, G.; Samor, B. *Trends Biotechnol.* **2006**, *24*, 235–243.
(2) (a) Konrad, M. W.; Bolonick, J. I. *J. Am. Chem. Soc.* **1996**, *118*, 10989–10994. (b) Williams, M. C.; Rouzina, I.; Bloomfield, V. A. *Acc. Chem. Res.* **2002**, *35*, 159–166. (c) Takahashi, M.; Lavery, R. *ChemPhysChem* **2009**, *10*, 1399–1404.
(3) For leading references into this large literature see: Zhang, L.; Peritz, A.; Meggers, E. *J. Am. Chem. Soc.* **2005**, *127*, 4174–4175; Ramaswamy, A.; Froeyen, M.; Herdewijn, P.; Ceulemans, A. *J. Am. Chem. Soc.* **2010**, *132*, 587–595.
(4) Nielsen, P. E.; Egholm, M.; Berg, R. H.; Buchardt, O. *Science* **1991**, *254*, 1497–1500; Egholm, M.; Behrens, C.; Christensen, L.; Berg, R. H.; Nielsen, P. E.; Buchardt, O. *J. Chem. Soc., Chem. Commun.* **1993**, *9*, 800–801.
(5) Egholm, M.; Buchardt, O.; Cristensen, R.; Behrens, C.; Frier, S. M.; Driver, D. A.; Berg, R. H.; Kim, S. K.; Nordén, B.; Nielsen, P. E. *Nature* **1993**, *365*, 566–568.
(6) Nielsen, P. E. *Curr. Opin. Biotechnol.* **1999**, *10*, 71–75.
(7) Nielsen, P. E. *Curr. Opin. Struct. Biol.* **1999**, *9*, 353–357.
(8) Mologni, L.; Nielsen, P. E.; Gambacorti-Passerini, C. *Biochem. Biophys. Res. Commun.* **1999**, *64*, 537–543.
(9) Koppelhus, U.; Nielsen, P. E. *Adv. Drug Delivery Rev.* **2003**, *55*, 267–280.
(10) Lundin, K. E.; Good, L.; Stroemberg, R.; Graeslund, A.; Smith, C. I. *Adv. Genet.* **2006**, *56*, 1–51; Pandey, V. N.; Upadhyay, A.; Chaubey, B. *Expert Opin. Biol. Ther.* **2009**, *9*, 975–989; Dragulescu-Andrasi, A.; Rapireddy, S.; He, G.; Bhattacharya, B.; Hyldig-Nielsen, J. J.; Zon, G.; Ly, D. H. *J. Am. Chem. Soc.* **2006**, *128*, 16104–16112; Sahu, B.; Chenna, V.; Lathrop, K. L.; Thomas, S. M.; Zon, G.; Livak, K. J.; Ly, D. H. *J. Org. Chem.* **2009**, *74*, 1509–1516.
(11) Cutrona, G.; Carpaneto, E. M.; Ulivi, M.; Roncella, S.; Landt, O.; Ferrarini, M.; Boffa, L. C. *Nat. Biotechnol.* **2000**, *18*, 300–303.
(12) Tonelli, R.; Purgato, S.; Camerin, C.; Fronza, R.; Bologna, F.; Alboresi, S.; Franzoni, M.; Corradini, R.; Sforza, S.; Faccini, A.; Shohet, J. A.; Marchelli, R.; Pession, A. *Mol. Cancer Ther.* **2005**, *4*, 779–783.
(13) Sen, S.; Nilsson, L. *J. Am. Chem. Soc.* **1998**, *120*, 619–631.
(14) Hatcher, E.; Balaeff, A.; Keinan, S.; Venkatramani, R.; Beratan, D. N. *J. Am. Chem. Soc.* **2008**, *130*, 11752–11761.
(15) Natsume, T.; Ishikawa, Y.; Dedachi, K.; Kurita, N. *Chem. Phys. Lett.* **2006**, *418*, 239–244.
(16) Tomac, S.; Sarkar, M.; Ratilainen, T.; Wittung, P.; Nielsen, P. E.; Nordén, B.; Graslund, A. *J. Am. Chem. Soc.* **1996**, *118*, 5544–5552.
(17) Nielsen, P. E. *Annu. Rev. Biophys. Biomol. Struct.* **1995**, *24*, 167–183.
(18) Wittung, P.; Nielsen, P. E.; Buchardt, O.; Egholm, M.; Nordén, B. *Nature* **1994**, *368*, 561–563.
(19) Rasmussen, H.; Kastrup, J. S.; Nielsen, J. N.; Nielsen, J. M.; Nielsen, P. E. *Nat. Struct. Biol.* **1997**, *4*, 98–101.
(20) Corradini, R.; Sforza, S.; Tedeschi, T.; Totsingan, F.; Marchelli, R. *Curr. Top. Med. Chem.* **2007**, *7*, 681–694.
(21) Menchise, V.; De Simone, G.; Tedeschi, T.; Corradini, R.; Sforza, S.; Marchelli, R.; Capasso, D.; Saviano, M.; Pedone, C. *Proc. Natl. Acad. Sci. U.S.A.* **2003**, *100*, 12021–12026.
(22) Sforza, S.; Haaima, G.; Marchelli, R.; Nielsen, P. E. *Eur. J. Org. Chem.* **1999**, *1*, 197–204.
(23) Sforza, S.; Corradini, R.; Ghirardi, S.; Dossena, A.; Marchelli, R. *Eur. J. Org. Chem.* **2000**, *16*, 2905–2913.
(24) Sforza, S.; Tedeschi, T.; Corradini, R.; Marchelli, R. *Eur. J. Org. Chem.* **2007**, *35*, 5879–5885.
(25) Wittung, P.; Eriksson, M.; Lyng, R.; Nielsen, P. E.; Nordén, B. *J. Am. Chem. Soc.* **1995**, *117*, 10167–10173.
(26) (a) Green, M. M.; Peterson, N. C.; Sato, T.; Teramoto, A.; Cook, R.; Lifson, S. *Science* **1995**, *268*, 1860–1866. (b) Green, M. M.; Park, J.-W.; Sato, T.; Teramoto, A.; Lifson, S.; Selinger, R. L. B.; Selinger, J. V. *Angew. Chem., Int. Ed.* **1999**, *38*, 3138–3154. (c) Green, M. M. *Circular Dichroism - Principles and Applications*, 2nd ed.; Berova, N., Nakanishi, K., Woody, R. W., Eds.; Wiley-VCH: Hoboken, NJ, 2000; Chapter 17.
(27) Rasmussen, H.; Liljefors, T.; Petersson, B.; Nielsen, P. E.; Kastrup, J. S. *J. Biomol. Struct. Dyn.* **2004**, *21*, 495–502.
(28) Pino, P.; Luisi, P. L. *J. Chim. Phys. Phys.-Chim. Biol.* **1968**, *65*, 130–139.
(29) Petersson, B.; Nielsen, B. B.; Rasmussen, H.; Larsen, I. K.; Gajhede, M.; Nielsen, P. E.; Kastrup, J. S. *J. Am. Chem. Soc.* **2005**, *127*, 1424–1430.
(30) Tedeschi, T.; Sforza, S.; Dossena, A.; Corradini, R.; Marchelli, R. *Chirality* **2005**, *17*, 196–204.
(31) Daniels, M.; Hart, L. P.; Ho, P. S.; Ballini, J. P.; Vigny, P.; Brochon, J. C. *Photochem. Photobiol. Sci.* **2007**, *6*, 883–893.
(32) Darrel, R., D. *Nucleic Acids Res.* **1995**, *23*, 5020–5026.
(33) Wei, C.; Jia, G.; Yuang, J.; Feng, Z.; Li, C. *Biochemistry* **2006**, *45*, 6681–6691.
(34) Alderfer, J. L.; Tazawa, I.; Tazawa, S.; Ts'o, P. O. P. *Biochemistry* **1974**, *13*, 1615–1622.
(35) Xodo, L.; Mancini, G.; Quadrifoglio, F.; Van der Marel, G.; Van Boom, J. *Nucleic Acids Res.* **1991**, *19*, 1505–1511.
(36) (a) Lawley, P. D. *Biochim. Biophys. Acta* **1956**, *21*, 481–483. (b) Tanaka, K.; Tengeiji, A.; Kato, T.; Namiki, T.; Toyama, N.; Shiro, M.; Shionoya, M. *J. Am. Chem. Soc.* **2002**, *124*, 12494–12498.
(37) He, W.; Hatcher, E.; Balaeff, A.; Beratan, D. N.; Gil, R. R.; Madrid, M.; Achim, C. *J. Am. Chem. Soc.* **2008**, *130*, 13264–13273.
(38) Haaima, G.; Rasmussen, H.; Schmidt, G.; Jensen, D. K.; Kastrup, J. S.; Wittung, S. P.; Nordén, B.; Buchardt, O.; Nielsen, P. E. *New J. Chem.* **1999**, *23*, 833–840.
(39) Eldrup, A. B.; Nielsen, B. B.; Haaima, G.; Rasmussen, H.; Kastrup, J. S.; Christensen, C.; Nielsen, P. E. *Eur. J. Org. Chem.* **2001**, *9*, 1781–1790.
(40) Nielsen, P. E., Ed.; *Peptide Nucleic Acids: Protocols and Applications*; Horizon Bioscience: Norwich, UK, 2004.
(41) Sasisekharan, V.; Pattabiraman, N.; Gupta, G. *Proc. Natl. Acad. Sci. U.S.A.* **1978**, *75*, 4092–4096.
(42) Naylor, L. H.; Yee, H. A.; Van de Sande, J. H. *J. Biomol. Struct. Dyn.* **1988**, *5*, 895–912.

(43) For one example and leading references see: Nonokawa, R.; Yashima, E. *J. Am. Chem. Soc.* **2003**, *125*, 1278–1283; For leading references into synthetic double helices see: Goto, H.; Katagiri, H.; Furusho, Y.; Yashima, E. *J. Am. Chem. Soc.* **2006**, *128*, 7176–7178.
(44) DeGreef, T. F. A.; Smulders, M. M. J.; Wolffs, M.; Schenning, A. P. H. J.; Sijbesma, R. P.; Meijer, E. W. *Chem. Rev.* **2009**, *109*, 5687−5754, for leading references.
(45) Fasel, R.; Parschau, M.; Ernst, K.-H. *Nature* **2006**, *439*, 449−452, for leading references.
(46) Green, M. M.; Zanella, S.; Gu, H.; Sato, T.; Gottarelli, G.; Jha, S. K.; Spada, G. P.; Schoevaars, A. M.; Feringa, B.; Teramoto, A. *J. Am. Chem. Soc.* **1998**, *120*, 9810–9817.
(47) Christensen, L.; Fitzpatrick, R.; Gildea, B.; Petersen, K. H.; Koch, T.; Egholm, M.; Buchardt, O.; Nielsen, P. E.; Coull, J. *J. Peptide Sci.* **1995**, *3*, 175–183.
(48) (a) Thomson, S. A.; Josey, J. A.; Cadilla, R.; Gaul, M. D.; Hassman, C. F.; Luzzio, M. J.; Pipe, A. J.; Reed, K. L.; Ricca, D. J.; Wiethe, R. W.; Noble, S. A. *Tetrahedron* **1995**, *51*, 6179–6194. (b) Breipohl, G.; Knolle, J.; Langner, D.; O'Malley, G.; Uhlmann, E. *Bioorg. Med. Chem. Lett.* **1996**, *6*, 665–670.
(49) Jain, V. Ph.D. Thesis, Polytechnic University, Brooklyn, NY, **2006**.
(50) (a) Crothers, D. M.; Kallenbach, N. R.; Zimm, B. H. *J. Mol. Biol.* **1965**, *11*, 802–820. (b) Applequist, J.; Damle, V. *J. Am. Chem. Soc.* **1965**, *87*, 1450–1458.